

Columnar dimer and plaquette resonating valence bond states of the quantum dimer model

P. W. Leung* and K. C. Chiu

*Department of Physics, Hong Kong University of Science and Technology
Clear Water Bay, Hong Kong*

Karl J. Runge

*Department of Physics, Lawrence Livermore National Laboratory, University of California
Livermore, California 94551*

(November 24, 2018)

We study the nature of the ground state of the quantum dimer model proposed by Rokhsar and Kivelson by diagonalizing the Hamiltonian of the model on square lattices of size $L \times L$, where $L \leq 8$, with periodic boundary conditions. Finite-size scaling studies of the columnar order parameter and the low lying excitation spectrum show no evidence of a dimer liquid state in any finite region of the zero temperature phase diagram. In addition, we find evidence of a transition from the columnar dimer state to an intermediate state at a negative value of V/J . This state is identified to be the plaquette resonating valence bond (RVB) state. The energy gap of this state vanishes as a power law of L . It exhibits columnar dimer order, but has disorder *within* the dimer columns. This state persists up to $V/J < 1$, and the system changes to a dimer liquid state only at $V/J = 1$.

PACS: 75.10Jm, 75.40Mg

I. INTRODUCTION

The quantum dimer model (QDM) was first introduced by Rokhsar and Kivelson (RK)¹. It was proposed as an alternative description of the non-Néel state of the spin- $\frac{1}{2}$ Heisenberg antiferromagnet on a square lattice. In a state with exponentially decaying spin-spin correlation and a large energy gap separating the spin excitations from the singlet ground state, RK argued that the low energy physics is contained in the “short-range resonating valence bond (RVB)” states, spanned by the set of nearest-neighbor valence bond states. Nearest-neighbor valence bonds are called dimers. The basis set thus consists of all possible dimer configurations at closest-packing (all sites form exactly one dimer with one of their nearest neighbors). RK also argued that the non-orthogonality of these basis states can be absorbed by defining a phenomenological Hamiltonian with short range dimer interactions. The relevance of this quantum dimer model to the frustrated quantum antiferromagnet was supported by other independent studies. Large- N expansion,² series expansion,³ and numerical diagonalization⁴ have shown that a spin-Peierls state exists in some region of the phase diagram where the Néel state is unstable. This spin-Peierls state corresponds to the state in the QDM where

the dimers are frozen into a columnar pattern (Fig. 1(a)). Recently the QDM has been generalized to the kagomé lattice by Zeng and Elser.⁵

The Hamiltonian of the QDM proposed by RK is

$$\mathcal{H} = \sum_{\text{plaquettes}} \left[-J \left(| \parallel \rangle \langle = | + \text{H.c.} \right) + V \left(| = \rangle \langle = | + | \parallel \rangle \langle \parallel | \right) \right]. \quad (1)$$

$| \parallel$ and $| =$ represent parallel dimers on the opposite sides of a square plaquette. The first term of \mathcal{H} is the dimer kinetic energy operator while the second term is the potential energy. The space spanned by all close-packed dimer configurations on a square lattice can be divided into distinct topological sections characterized by a pair of conserved winding numbers (Ω_x, Ω_y) (refer to Appendix A). On an $L \times L$ square lattice, the allowed winding numbers are $-L/2 \leq \Omega_x, \Omega_y \leq L/2$. At $V/J > 1$, the exact ground state of the QDM is the staggered dimer solid shown in Fig. 1(b). It is four-fold degenerate and has winding numbers $(\pm L/2, 0)$ and $(0, \pm L/2)$. At $V/J \ll -1$, the ground state develops columnar order as shown in Fig. 1(a). At $V/J = 1$, the lowest energy states in all topological sectors are zero-energy eigenstates of \mathcal{H} . They are equal superpositions of all the dimer configurations in their sectors. Therefore, the ground state at $V/J = 1$ is a dimer liquid, and any ground state dimer correlation function can be calculated exactly by the method of Fisher and Stephenson⁶ for the classical dimer problem. Consequently this state is called the FS state. The ground state properties of the QDM in the range $0 \leq V/J < 1$ are not so clear. There are three main questions: (a) is the ground state in this range ordered (dimer solid) or disordered (dimer liquid)? (b) If it is ordered, what is the nature of this order? And (c) if it is disordered, is there a gap in the low lying excitation spectrum? RK suggested that a dimer liquid state can exist in a finite region of $V/J < 1$. By numerically diagonalizing the QDM on square lattices up to 6×6 , Sachdev⁷ found evidence for the columnar state, but no evidence for a dimer liquid state at $V/J \neq 1$. However, due to finite-size effects, he did not rule out the possibility that dimer liquid exists over a finite range $\kappa < V/J \leq 1$, and

estimated a lower bound $0.5 < \kappa$. On the other hand, some analytic studies have suggested the existence of a dimer liquid state at $V/J \neq 1$. By mapping the QDM to a roughening problem, Levitov⁸ showed that a dimer liquid with gapless excitations may exist. Orland⁹ formulated the QDM as a system of non-interacting fermionic strings, and showed that at $V/J = 0$, the ground state is a dimer liquid. From this he inferred that the ground state is a dimer liquid for $0 \leq V/J \leq 1$, with a phase transition to a dimer solid at some $V/J < 0$. We also note that another kind of dimer order has been proposed,¹⁰ although in a different context. This is a plaquette RVB state as shown in Fig. 1(c), where every other plaquette is in the $|\parallel\rangle$ or $|\Rightarrow\rangle$ state with equal probability and independent of other plaquettes. In this paper, we extend Sachdev's calculations to an 8×8 square lattice. We aim to identify the different phases of the QDM in the range $V/J < 1$.

II. NUMERICAL CALCULATIONS

Using the Lanczos algorithm, we diagonalize the Hamiltonian \mathcal{H} in the range $-1 < V/J < 1$ on an $L \times L$ square lattice with periodic boundary conditions, where $L = 4, 6$, and 8 . The basis states are all possible dimer configurations at closest packing. The number of basis states for a given L can be evaluated⁶ analytically. Enumerating all the dimer configurations is much more difficult. Nevertheless, we have devised an efficient algorithm which enumerates all the 300 million dimer configurations on the $L = 8$ lattice within four hours using an HP 735 workstation (see Appendix B). Using translational symmetry, we can reduce the number of basis states on an $L \times L$ lattice by a factor of about L^2 . For $V/J < 1$, the ground state has momentum $\mathbf{k} = (0, 0)$, and winding numbers $(0, 0)$. By restricting the basis states to the topological sector with winding numbers $(0, 0)$, the number of basis states can be further reduced by a factor of about 2. To calculate the ground state eigenvector, we restrict ourselves to the subspace with momentum $\mathbf{k} = (0, 0)$ and winding numbers $(0, 0)$. The number of basis states in this subspace is about 2.4 million. This makes the numerical diagonalization possible on a workstation.

III. SYMMETRIES OF LOW LYING EXCITED STATES

To study the different phases in the range $-1 < V/J < 1$, we first study the symmetries of the low lying excited states. They are important in finite-size studies. If a system possesses a broken symmetry in the thermodynamic limit, the ground state of the finite system will still be totally symmetric. In this case the ground state expectation of the appropriate order parameter will have long-

range correlations, and there will exist low lying excited states with the appropriate symmetries. The columnar dimer state shown in Fig. 1(a) has winding numbers $(0, 0)$ and is four-fold degenerate. These degenerate states can be combined to form four states, two with momentum $(0, 0)$, and two with momenta $(\pi, 0)$ and $(0, \pi)$. Consequently in a finite system which possesses columnar order in the thermodynamic limit, the state with momentum $(0, 0)$ will be the ground state and the others will appear as low lying excited states, which are degenerate with the ground state in the thermodynamic limit. Note that the same is true for the plaquette RVB state shown in Fig. 1(c). Therefore, low lying excited states with momenta $(\pi, 0)$ and $(0, \pi)$ may indicate that columnar or plaquette RVB order exists in the ground state.

We calculate the energies of the lowest few eigenstates of the QDM on the $L = 4, 6$ and 8 lattices for $-1 \leq V/J < 1$. All three lattices show qualitatively the same picture. The ground state E_0 always has zero momentum and winding numbers, as mentioned in section II. Except when V/J is close to 1, the first excited state is degenerate with momenta $(\pi, 0)$ and $(0, \pi)$, and has zero winding numbers. We call this state $E_{(\pi, 0)}$. In the same region, the next excited state is degenerate with momenta $(0, 0)$ and (π, π) , and has winding numbers $(\pm 1, 0)$ and $(0, \pm 1)$. We call this state $E_{(\pi, \pi)}$. In Fig. 2 we plot the energies of the states E_0 , $E_{(\pi, 0)}$ and $E_{(\pi, \pi)}$ in a small range of V/J close to 1 for the $L = 8$ system. We can see that there exist a δ_L (which depends on the size L) close to but less than 1, such that at $V/J = \delta_L$, $E_{(\pi, \pi)}$ and $E_{(\pi, 0)}$ cross each other and $E_{(\pi, \pi)}$ becomes the first excited state for $\delta_L < V/J < 1$. This crossing of energy levels may imply the existence of a new ground state in the region $\delta_L < V/J < 1$. However, finite-size extrapolation analysis on δ_L shows that this is not the case. As shown in Fig. 3, δ_L approaches 1 as a power law of L ,¹¹

$$(1 - \delta_L) \propto L^{-2.13}. \quad (2)$$

In other words, such a spurious energy level crossing is only a finite-size effect. It does not occur in the thermodynamic limit and no transition is likely to occur at V/J close to 1. Therefore, we expect that the $E_{(\pi, 0)}$ state is always the lowest excited state in the range $-1 \leq V/J < 1$. This is consistent with, but does *not* imply, the existence of long-range order (LRO) in the QDM at $-1 \leq V/J < 1$.

Next we study the energy gap ΔE_L , which is the energy difference between $E_{(\pi, 0)}$ and E_0 . Fig. 4 shows different plots of ΔE_L vs L at different V/J . When V/J is close to 1, complication arises because of the spurious crossing over of the states $E_{(\pi, 0)}$ and $E_{(\pi, \pi)}$ at δ_L . But we find that ΔE_L is not very sensitive to V/J in the region close to δ_L (see Fig. 2). Consequently we plot ΔE_L at $V/J = \delta_L$ (instead of at the same V/J for different L) when V/J is close to 1. From Fig. 4 we can clearly distinguish two different behaviors. At $V/J = -1$, ΔE_L decays exponentially with L . This is a clear signal for

the existence of LRO. When $0 \leq V/J < 1$, we find that ΔE_L vanishes with a power law in L . Best fit to the data shows that the power is approximately 2 in the whole range. For $-1 < V/J < 0$, we are not able to determine whether ΔE_L has exponential or power law dependence on L . This is probably because of the more serious finite-size effect when V/J is close to a transition point. Hence we infer that there are two phases in the range $-1 \leq V/J < 1$. At some negative V/J , a transition occurs and the dependence of ΔE_L on L changes from exponential to power law.

IV. COLUMNAR ORDER PARAMETER

The columnar dimer order parameter is defined as⁷

$$\Psi_{col}(\mathbf{r}) = (-1)^{r_x} \left[n(\mathbf{r} + \frac{\hat{\mathbf{x}}}{2}) - n(\mathbf{r} - \frac{\hat{\mathbf{x}}}{2}) \right] + i (-1)^{r_y} \left[n(\mathbf{r} + \frac{\hat{\mathbf{y}}}{2}) - n(\mathbf{r} - \frac{\hat{\mathbf{y}}}{2}) \right], \quad (3)$$

where $\hat{\mathbf{x}}$ and $\hat{\mathbf{y}}$ are unit vectors. The dimer number operator $n(\mathbf{r} + \frac{\hat{\mathbf{e}}}{2})$ is 1 if the site at \mathbf{r} and its nearest neighbor at $\mathbf{r} + \hat{\mathbf{e}}$ form a dimer, and zero otherwise. In the finite-size study, one defines the order parameter⁷

$$\chi_L^2 = \left\langle \left| \frac{1}{L^2} \sum_{\mathbf{r} \in A} \Psi_{col}(\mathbf{r}) \right|^2 \right\rangle. \quad (4)$$

For a dimer liquid which has no long-range dimer order, χ_L is zero in the large L limit. If long-range columnar order exists, χ_L remains finite at large L . In Fig. 5 we plot χ_L versus V/J . When V/J is close to -1 , χ_L is approximately linear in $1/L^2$. But when V/J is increased, a linear relation in $1/L$ fits the data better. Unfortunately we are not able to determine the point where these two behaviors change from one to another. Using these linear relations, we extrapolate χ_L to obtain χ_∞ , which is also plotted in Fig. 5. It shows that χ_∞ is finite at $V/J < 1$, which signifies the existence of columnar order. χ_∞ decreases as V/J approaches 1, showing that the columnar order is weakening. But there is no evidence that χ_∞ is zero at any $V/J < 1$. χ_∞ clearly shows that the columnar order persists for $V/J < 1$.

Different dependence of χ_L on L ($\propto 1/L^2$ and $1/L$) may imply different orders in the respective regions. One defines the correlation function of Ψ_{col} ,⁷

$$G(\mathbf{r}) = \langle \Psi_{col}^*(\mathbf{r}_1) \Psi_{col}(\mathbf{r}_1 + \mathbf{r}) \rangle, \quad (5)$$

where \mathbf{r}, \mathbf{r}_1 are in the A sublattice. In the two regions where χ_L has finite-size corrections $1/L^2$ and $1/L$, $G(r)$ probably decays exponentially and as a power law in r , respectively, to a non-zero constant value. Fig. 6 shows $G(r)$ in the $L = 8$ system. Unfortunately, direct observation of how $G(r)$ decays with r is not possible in this system size. Fig. 6 shows that when V/J is away from 1,

$G(r)$ is a nonzero constant at large r . When V/J is close to 1, it is not possible to tell from Fig. 6 whether $G(r)$ is small or zero at large r . Nevertheless, it tells us that in the range $-1 \leq V/J < 1$ the long-range order, if exists, should be columnar.

As suggested in Ref. 7, a further probe of the columnar dimer order is provided by the cumulant of the columnar order parameter,

$$g_L = \left\langle \left| \sum_{\mathbf{r}} \Psi_{col}(\mathbf{r}) \right|^4 \right\rangle / \left\langle \left| \sum_{\mathbf{r}} \Psi_{col}(\mathbf{r}) \right|^2 \right\rangle^2. \quad (6)$$

If long-range columnar dimer order exists, $g_L \rightarrow 1$ as $L \rightarrow \infty$. We plot g_L versus V/J in Fig. 7(a). Standard finite-size scaling theory¹² shows that at phase transition, g_L at different L cross at a unique point. Since g_L do not cross except when V/J is close to 1, Fig. 7(a) tells us that the order parameter Ψ_{col} detects no transition except when V/J is close to 1. This is the transition to the dimer liquid (FS) state. Since our system size L is not large enough to make g_L cross at one point, it is not possible to determine the transition point from Fig. 7(a). Nevertheless, our previous finite-size analysis of ΔE_L and χ_L strongly suggest that some kind of columnar LRO persists all the way up to $V/J = 1$. We also note that g_L detects no transition at any $-1 \leq V/J < 0$, in contrary to the results of ΔE_L and χ_L .

V. DISORDER WITHIN THE COLUMNS

It is easy to understand why g_L is not able to detect the transition at $V/J < 0$. Note that in the plaquette RVB state, χ_L is also non-zero in the large L limit. It can be considered as a state which possesses long-range ‘‘columnar order’’ (as measured by χ_L), but has disorder within the established columns. To detect this disorder we introduce an order parameter $M_{\parallel,=}$,

$$M_{\parallel,=} = \frac{1}{L^2} \sum_{\text{plaquettes}} \left[n(| \parallel \rangle) - n(| = \rangle) \right], \quad (7)$$

where $n(| \parallel \rangle)$ and $n(| = \rangle)$ are number operators of vertical (\parallel) and horizontal ($=$) dimer pairs respectively. In the perfect columnar state, $|M_{\parallel,=}| = 1/2$, while in the plaquette RVB, dimer liquid and the staggered state, $M_{\parallel,=} = 0$. Analogous to Ψ_{col} , we define the cumulant

$$g_{\parallel,=} = \frac{\langle |M_{\parallel,=}|^4 \rangle}{\langle |M_{\parallel,=}|^2 \rangle^2}. \quad (8)$$

Again, finite-size scaling theory shows that at the phase transition, $g_{\parallel,=}$ at different L should intersect at a unique point. In Fig. 7(b) we plot $g_{\parallel,=}$ vs V/J for different L . Although the three curves do not intersect at a single point, the crossing of the curves at $L = 6$ and 8 indicates that a transition is possible at some negative value of

V/J . This is consistent with the results of ΔE_L and χ_L . We are not able to obtain a good estimation for the transition point V_c/J . But very roughly, $V_c/J \sim -0.2$.

We also calculate the moments of $M_{|,-}$,

$$M_{|,-} = \frac{1}{L^2} \sum_{\text{plaquettes}} \left[n(|) - n(-) \right], \quad (9)$$

i.e. the difference between the number of vertical and horizontal dimers. The corresponding cumulant $g_{|,-}$ is shown in Fig. 7(c). We find a similar crossing of $g_{|,-}$ for $L = 6, 8$ also near $V/J \sim -0.2$. Both $M_{|,-}$ and $M_{||,=}$ should be probes of the same ordered columnar to plaquette RVB transition. We note that for $V > V_c$ both $g_{||,=}$ and $g_{|,-}$ are close to 3. This value is the expected gaussian moment ratio for disordered states. This strongly suggests there is no $M_{||,=}$ or $M_{|,-}$ LRO for the whole range of $V > V_c$. For $V/J < -1$ the cumulants approach 1 for the ordered columnar state. In the $L \rightarrow \infty$ limit the cumulants should become 1 for all $V < V_c$. Fig. 7(b) and (c) are consistent with this scenario.

VI. DIMER CORRELATIONS

$g_{||,=}$ and $g_{|,-}$ show that the possible transition at V_c/J is between two states with long-range columnar order, but one has disorder within the columns. Next we are going to study the dimer correlations in these two states. The spatial correlation of the dimers can be displayed by evaluating the dimer-dimer correlation function,¹³

$$C_{(ij)(kl)} = \frac{\langle n_{ij} n_{kl} \rangle - \langle n_{ij} \rangle^2}{\langle n_{ij}^2 \rangle - \langle n_{ij} \rangle^2}, \quad (10)$$

where $n_{ij} \equiv n(\frac{1}{2}(\mathbf{r}_i + \mathbf{r}_j))$. If the dimers do not have LRO, $C_{(ij)(kl)}$ should show some short-range correlations, and fall off rapidly as the separation between the bonds (ij) and (kl) increases. On the other hand, if the dimers have LRO, $C_{(ij)(kl)}$ should reflect the pattern of the long-range correlations. Fig. 8 shows the dimer-dimer correlation in the $L = 8$ system at $V/J = -1$ and 0. The reference bond (ij) is represented by a double line. $C_{(ij)(kl)}$ is proportional to the thickness of the line joining the pair of sites k and l . Solid line means $C_{(ij)(kl)} > 0$ (correlation), and broken line means $C_{(ij)(kl)} < 0$ (anti-correlation). It is obvious that in both cases the overall order is columnar — those bonds with positive $C_{(ij)(kl)}$ are arranged in well-defined columns. This is consistent with the study using $\Psi_{col}(\mathbf{r})$ as the order parameter (Sec. IV). Except for the trivial short-range correlations, $C_{(ij)(kl)}$ does not fall off significantly with distance. This is an indication that the correlation is long-range. A major difference between Fig. 8(a) and (b) is that in the latter, $C_{(ij)(kl)}$ for vertical (kl) are very close to zero, except for those in contact with (ij) . In the perfect columnar state as shown in Fig. 1(a), $C_{(ij)(kl)} = 1$ or $-1/3$ when the bond

(kl) forms and does not form dimer respectively. (Here the reference bond (ij) has been chosen to be one of the horizontal bonds that form dimer in Fig. 1(a).) This is to be compared to the result at $V/J = -1$ (Fig. 8(a)). In the perfect plaquette RVB state as shown in Fig. 1(c), except for those (kl) which are in the same plaquette as (ij) , $C_{(ij)(kl)} = 0$ for vertical (kl) , and $C_{(ij)(kl)} = \pm 1/3$ for horizontal (kl) , depending on whether (kl) belongs to any one of the plaquettes shown in Fig. 1(c). In the same plaquette as (ij) , horizontal and vertical (kl) have $C_{(ij)(kl)} = 2/3$ and $-1/3$ respectively. This is to be compared to the result at $V/J = 0$ (Fig. 8(b)). Hence the dimer correlations strongly suggest that at $V/J = -1$, the ground state is ordered columns, whereas at $V/J = 0$, it is the plaquette RVB state.

VII. PLAQUETTE RVB STATE AND THE TRANSITION AT V_c/J

From the above results and discussions, there is evidence that at V_c/J , the ground state of the QDM changes from the ordered columnar to the plaquette RVB state. Since this transition does not appear to have been discussed in the literature, we will discuss it in a little more detail. One can motivate the existence of this transition by a simple argument where the QDM is approximately mapped onto a two-dimensional Ising model in a transverse field. The $T = 0$ transition from ferromagnet to paramagnet in that model corresponds to the $V_c/J < 0$ transition of the QDM discussed in the previous sections. We now outline the steps and implications of this approximate treatment.

First consider the case $V/J \ll -1$ where the system tends to the ordered columnar state in Fig. 1(a). The basic quantum fluctuations in the ground state are induced by the kinetic energy term in (1), namely by flipping $|\Rightarrow$ to $|\parallel\rangle$. For each dimer populated column in Fig. 1(a) consider *every other* plaquette (as in Fig. 1(c)) to have an index “ i ” and state variable $\sigma_i^z = 1$ if it is in the state $|\Rightarrow$ and $\sigma_i^z = -1$ if it is $|\parallel\rangle$. Fig. 1(a) has all $\sigma_i^z = 1$, *i.e.* a ferromagnetic arrangement, whereas Fig. 1(c) has all $\sigma_i^z = \pm 1$ with probability 1/2, *i.e.* a paramagnetic arrangement. Note also that the other ferromagnetic Ising configuration, with all $\sigma_i^z = -1$, gives another perfectly ordered columnar state. The collection of states generated by all possible $\{\sigma_i^z\}$ is, of course, a small subset of the set of all close-packed dimer configurations. However, they at least describe the plaquette RVB states, the ordered columnar states, and one half of the basic flipping excitations. Given that our earlier numerical results suggest columnar order for all $V/J < 1$, we do not worry too much that the $\{\sigma_i^z\}$ subset of dimer states are, by construction, *constrained* to have long-range columnar order, since we are concerned with the disordering of other degrees of freedom (*e.g.* dimer pair arrangements and correlations within each established column).

Limiting the system to the collection of all possible $\{\sigma_i^z\}$ values, one can show that the Hamiltonian of the QDM is, to within an additive constant,

$$\mathcal{H} = -J \sum_i \sigma_i^x + \frac{V}{4} \sum_{\langle ij \rangle} \sigma_i^z \sigma_j^z, \quad (11)$$

where the sums are over every other plaquette as shown in Fig. 1(c). σ_i^x and σ_i^z are Pauli operators. The kinetic energy term with J now induces flipping of the σ^z variables (like a transverse Ising field h_x), and the potential energy term V introduces interactions (like an Ising exchange integral \mathcal{J}_z) between neighboring plaquettes as shown in Fig. 1(c).¹⁴

For $V/J \ll -1$ all the σ_i^z are arranged ferromagnetically, whereas for some $V_c/J < 0$ the system undergoes a continuous phase transition (in the universality class of the classical 3D Ising model) to a state with no LRO in the σ_i^z variables. Indeed, the case $V = 0$ is trivially seen to be perfectly disordered with respect to the σ_i^z variables, and is precisely the state represented schematically in Fig. 1(c). For $V_c < V < 0$ there is some short ranged σ^z order, but no LRO. Since our (=) (||) pairs of dimers are neither allowed to break apart nor to move to neighboring plaquettes, this approximation has long-range columnar order (as measured by Ψ_{col}) preserved past the transition point V_c . Our numerical data suggests this to be the case for the QDM as well: LRO in Ψ_{col} exists for all $V/J < 1$ but there is a loss of LRO in $M_{||,=}$ at some negative value of V .

One may speculate that the $V/J < 0$ transition in the QDM is also in the same universality class of the 3D Ising model. Unfortunately the system sizes we can deal with are too small to determine V_c accurately, let alone to estimate the critical exponents.

VIII. FINITE TEMPERATURE PHASE DIAGRAM

Although our numerical calculations are limited to the $T = 0$ ground state of the QDM, it is interesting to speculate on the behavior of the system at finite temperatures. The simplest, and we feel most likely, scenario is displayed schematically in Fig. 9. For any fixed ratio V/J , as $T \rightarrow \infty$ the only interaction that matters is the hard-core dimer constraint, and so the FS dimer liquid will always be obtained at high enough temperature. We expect that for fixed $V < V_c$ as T is increased the ordered columnar state will give way to a plaquette RVB state,¹⁵ and at a second higher temperature the columnar order will be destroyed as the system enters the high-temperature dimer liquid phase. Similarly, for $V > J$ the staggered phase in Fig. 1(b) will be destroyed at high enough T . The simplest guess is that it goes directly to the dimer liquid,¹⁶ although it is not possible to rule out other phases. It seems likely that the high temperature dimer liquid region makes it all the way down

to the $T = 0$ axis, but only at the point $V = J$. It is intriguing that the $T = \infty$ Fisher-Stephenson (FS) state is *exactly* regained at $T = 0$ at a single point.

IX. CONCLUSION

To conclude, we find no evidence of a dimer liquid state in the QDM in the range $-1 \leq V/J < 1$. In this range, the QDM exists in two states. At $-1 \leq V/J < V_c/J$, the ground state possesses long-range columnar dimer order as suggested in Fig. 1(a). Its columnar order correlation function $\langle \Psi_{col}(0) \Psi_{col}(\mathbf{r}) \rangle$ is likely to decay to a constant value exponentially with r , and it has exponentially vanishing energy gap. This state should exist at any $V/J \leq -1$, because negative V favors parallel dimers. At $V_c/J < V/J < 1$, the ground state is the plaquette RVB state as illustrated in Fig. 1(c). Its columnar order correlation $\langle \Psi_{col}(0) \Psi_{col}(\mathbf{r}) \rangle$ is likely to decay to a constant value as a power law of r , and the energy gap vanishes as a power of L . By approximately mapping the QDM to an Ising model with a transverse field, we infer that the transition at V_c/J is continuous and possibly in the same universality class as the 3D classical Ising model. Unfortunately, our system sizes do not allow us to determine the precise value of V_c/J . Our rough estimate is $V_c/J \sim -0.2$. We note that we cannot rule out additional transitions in the range $V_c/J < V/J < 1$, we can only say the quantities we have measured do not indicate any more.

Compared to earlier work⁷ which concluded that a dimer liquid state *may* exist in $\kappa \leq V/J \leq 1$ and gave an upper bound of 0.5 to κ , we are able to perform more reliable finite-size scaling analysis with the addition of the $L = 8$ results. Our results push κ to very close to 1 which suggest that κ is in fact 1. Note that although our results disagree with Ref. 9, our conclusions have something in common. Ref. 9 claims that the QDM is a dimer liquid at $V/J = 0$, and exhibits a transition from the columnar to the dimer liquid state at some negative V/J . We also find a transition at some negative V/J .¹⁷ However, this transition is not from the columnar to dimer liquid state, but rather to an intermediate state which we identify to be the plaquette RVB state.

ACKNOWLEDGMENTS

PWL thanks C. Zeng for very useful discussions, and C. L. Henley for communicating his results before publication. This work was supported in part by Hong Kong RGC grant HKUST619/95P.

APPENDIX A: WINDING NUMBERS

Following Ref. 1 we use the columnar state as the reference configuration to define the winding numbers. In Fig. 10(a), the dimers of such a reference configuration are indicated by dash lines. The arrows along the dimers always point from the A sublattice (solid circles) to the B sublattice (open circles). In Fig. 10(b), a dimer configuration (indicated by solid lines) is superimposed on the reference configuration, but the arrows along the dimers (solid lines) point from the B sublattice to the A sublattice. This results in directed close paths which may wrap around the boundaries (with periodic boundary conditions). The winding numbers Ω_x and Ω_y are the net number of loops (clockwise minus counterclockwise) wrapping around the boundaries in the x and y directions respectively. Each dimer configuration has a unique pair of winding numbers. By repeatedly flipping parallel dimer pairs (i.e., applying \mathcal{H}) of a dimer configuration, one can generate all dimer configurations with the same winding numbers. But no two configurations with different winding numbers are related by such dimer flipping operations. Therefore, the Hilbert space spanned by all close-packed dimers can be divided into subspaces labelled by winding numbers.

To calculate the winding numbers of a given dimer configuration, we start from a site and traverse the lattice following the arrows as described above until we return to the starting site. We mark all the sites along this path and count the net number of times it crosses the boundaries in the x and y directions. This procedure is repeated starting from an unmarked site until all sites are marked. It is easy to see that the columnar dimer state in Fig. 1(a) has winding numbers $(0, 0)$, and the staggered state in Fig. 1(b) has winding numbers $(\pm L/2, 0)$.

APPENDIX B: ENUMERATING DIMER CONFIGURATIONS

In this Appendix we describe the way we generate all the close-packed dimer configurations on an $L \times L$ lattice. Again we divide the square lattice into two sublattices A and B . At close-pack, each site is one end of exactly one dimer. Consequently, a dimer configuration can be represented by specifying the direction ($\pm \hat{x}$ or $\pm \hat{y}$) of the dimer attached to each site in the A sublattice. There are 2^{L^2} such combinations. But most of them are forbidden because some sites in the B sublattice have zero or more than one dimer attached. The most straightforward way to enumerate all the dimer configurations is to scan through these 2^{L^2} combinations to identify the allowed configurations. But this takes prohibitively long for $L = 8$. We need a clever way to identify and eliminate the forbidden configurations quickly.

We further divide the A sublattice into two quarter-lattices A_0 and A_1 . Each site takes up two bits in a

computer word, with the four binary values 00, 01, 10, and 11 representing the direction of the dimer attached to it. We divide our task into two steps. First we generate allowed configurations for A_0 alone, without considering A_1 . Then we generate the allowed configurations for A_1 under the constraints of the A_0 configurations. The A_0 and A_1 configurations together give all the allowed dimer configurations.

A_0 has $L^2/4$ sites. Each A_0 configuration is represented in the computer by an integer word with at least $2 \times (L^2/4) = L^2/2$ bits. The $2j$ th and $2j + 1$ th bits of the integer word represent the direction of the dimer attached to the j th site of A_0 . In this way each A_0 configuration is uniquely associated with an integer value. To scan through all the possible A_0 configurations, we start from an integer value $2^{L^2/2} - 1$ whose binary representation has 1s in the lower $L^2/2$ bits, and 0s otherwise. This integer value corresponds to the A_0 configuration with all dimers pointing in the same direction. Successively decreasing this integer value by 1 is equivalent to rotating the dimers in all possible directions starting from the 0th, 1st, ... sites. In this way all possible A_0 configurations can be generated. For each integer value (i.e., possible A_0 configuration), we check for conflict starting from the last site. If at some stage we find that the dimers attached to the i th and j th sites ($i > j$) of A_0 are conflicting (both connect to the same site in the B sublattice), we can skip all the bits lower than the $2j$ th bit, i.e., instead of decrementing the integer value by 1, we can go to the next possible configuration by changing the $2j$ th and $2j + 1$ th bits. This substantially decreases the run time. For $L = 8$, A_0 has 9 983 558 allowed configurations.

The set of allowed configurations for A_1 is the same as that for A_0 . Naively we can match these two sets of configurations and eliminate the forbidden ones. But this involves $(9\,983\,558)^2 \sim 10^{14}$ steps for $L = 8$ and will take prohibitively long. We must fully utilize the geometrical constraints imposed by the A_0 configurations when enumerating the possible A_1 configurations. For a particular A_0 configuration, we mark the allowed dimer directions for each site in A_1 under the constraints imposed by that A_0 configuration. The total number of combinations is substantially smaller than $2^{L^2/2}$. We then scan through all these combinations in the same manner as in enumerating the A_0 configurations. Repeating the same procedure generates all the allowed dimer configurations. For $L = 4, 6,$ and 8 , the number of allowed dimer configurations are 272, 90 176, and 311 853 312 respectively. For $L = 8$, all the allowed dimer configurations can be enumerated in about four hours using an HP 735 workstation.

* Electronic address: phleung@usthk.ust.hk

- ¹ D. Rokhsar and S. Kivelson, Phys. Rev. Lett. **61**, 2376 (1988).
- ² N. Read and S. Sachdev, Nucl. Phys. B **316**, 609 (1989); Phys. Rev. Lett. **62**, 1694 (1989); S. Sachdev and N. Read, Int. J. Mod. Phys. B **5**, 219 (1991).
- ³ M. P. Gelfand, R. R. P. Singh, and D. A. Huse, Phys. Rev. B **40**, 10801 (1989).
- ⁴ P. W. Leung and N. Lam, Phys. Rev. B **53**, 2213 (1996).
- ⁵ C. Zeng and V. Elser, Phys. Rev. B **51**, 8318 (1995).
- ⁶ M. E. Fisher and J. Stephenson, Phys. Rev. **132**, 1411 (1963).
- ⁷ S. Sachdev, Phys. Rev. B **40**, 5204 (1989).
- ⁸ L. S. Levitov, Phys. Rev. Lett. **64**, 92 (1990).
- ⁹ P. Orland, Phys. Rev. B **49**, 3423 (1994).
- ¹⁰ M. E. Zhitomirsky and K. Ueda, *unpublished*.
- ¹¹ This power law behavior has been predicted using a “height analysis” of the QDM, C. L. Henley, private communications.
- ¹² K. Binder, *Finite Size Scaling and Numerical Simulation of Statistical Systems*, Ed. V. Privman (World Scientific, Singapore, 1990).
- ¹³ P. W. Leung and V. Elser, Phys. Rev. B **47**, 5459 (1993).
- ¹⁴ We note that if the “expansion” is performed about staggered columns (every other dimer column shifted by one plaquette) additional terms proportional to $V \sum \sigma_i^z$ will appear in \mathcal{H} , but this does not change our conclusions that a disordering transition occurs for some $V/J < 0$.
- ¹⁵ Recalling our simple transverse Ising model description, this $T > 0$ transition to plaquette RVB state should be in the 2D classical Ising model, not 3D. Even if the transverse Ising picture breaks down, it should be generally true that the quantum phase transition of the QDM at $T = 0$, $V = V_c$ is in a 2+1 dimensional classical system universality class, while the rest of the $T > 0$ critical line is in some 2-dimensional system universality class.
- ¹⁶ The substantial difference in symmetry and winding numbers between the staggered phase and the dimer liquid may mean that the transition between them is first-order.
- ¹⁷ Indeed, our analysis cannot rule out $V_c = 0$.

FIG. 1. The (a) columnar, (b) staggered, and (c) plaquette RVB states.

FIG. 2. Energy levels E_0 , $E_{(\pi,0)}$, and $E_{(\pi,\pi)}$ for the $L = 8$ system. All other energy levels are higher than these three and are not shown.

FIG. 3. $(1 - \delta_L)$ vs L . The straight line is the best fit to the data, $1 - \delta_L = 3.1544 L^{-2.13}$.

FIG. 4. (a) ΔE_L vs L in semi-logarithmic scale. The straight line is the best fit to the data, $\Delta E_L = 2.742 e^{-0.511L}$. (b) Similar plot but in logarithmic scale. δ_L is close to 1 (see Fig. 3). The straight lines are best fits to the data of the form $\Delta E_L \propto 1/L^2$.

FIG. 5. χ_L vs V/J for $L = 4, 6, 8$. \triangle and ∇ are χ_∞ obtained by extrapolating χ_L linearly in $1/L^2$ and $1/L$ respectively.

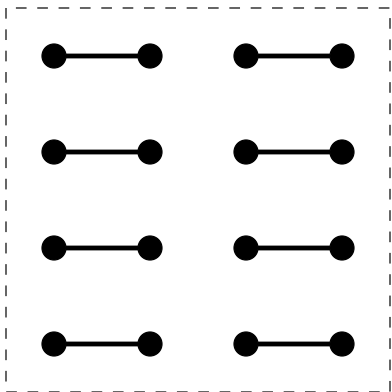
FIG. 6. $G(r)$ at different V/J for $L = 8$.

FIG. 7. Various cumulants vs V/J for $L = 4, 6$, and 8. (a) g_L , (b) $g_{||,=}$, and (c) $g_{||,-}$.

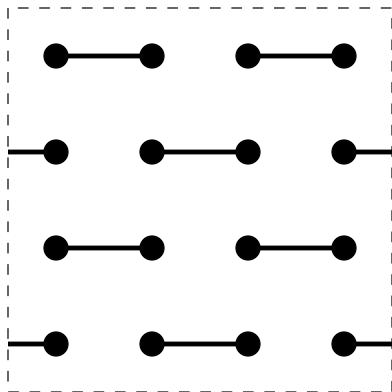
FIG. 8. Dimer-dimer correlation $C_{(ij)(kl)}$ in the $L = 8$ system at (a) $V/J = -1$ and (b) $V/J = 0$. Only a quadrant of the system containing all the inequivalent dimer pairs is shown. The reference bond (ij) is represented by a double line. $C_{(ij)(kl)}$ is proportional to the thickness of the line joining the pair of sites k and l . Solid line means $C_{(ij)(kl)} > 0$, and broken line means $C_{(ij)(kl)} < 0$. Note that the line widths are in the same scale in both cases. The values of $C_{(ij)(kl)}$ are shown next to the bonds, where different fonts are used for vertical and horizontal bonds.

FIG. 9. Speculated phase diagram of the QDM.

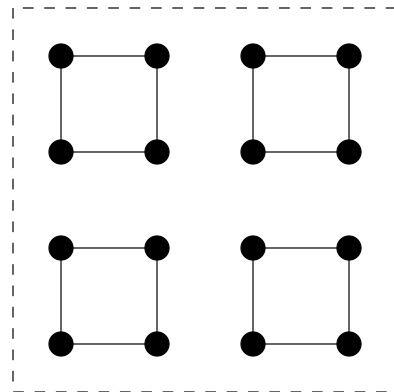
FIG. 10. (a) The reference columnar dimer configuration, with arrows pointing along the dimers from the A sublattice (\bullet) to the B sublattice (\circ). (b) A dimer configuration (indicated by solid lines) superimposed on (a), but with arrows pointing in the opposite direction, i.e., from the B sublattice (\circ) to the A sublattice (\bullet). This dimer configuration has winding numbers $(0, 1)$ or $(0, -1)$.



(a)



(b)



(c)

Fig. 1

Fig. 2

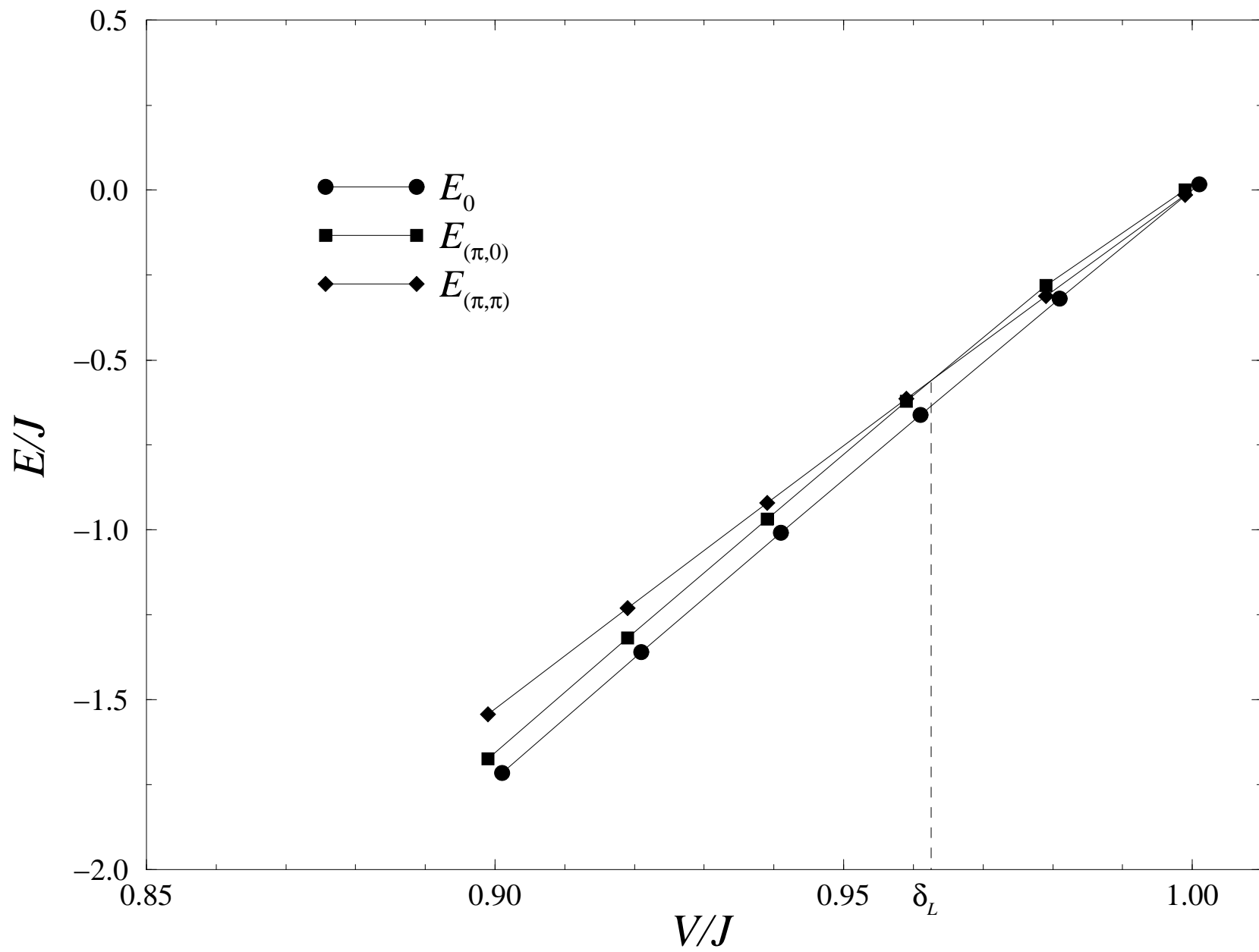


Fig. 3

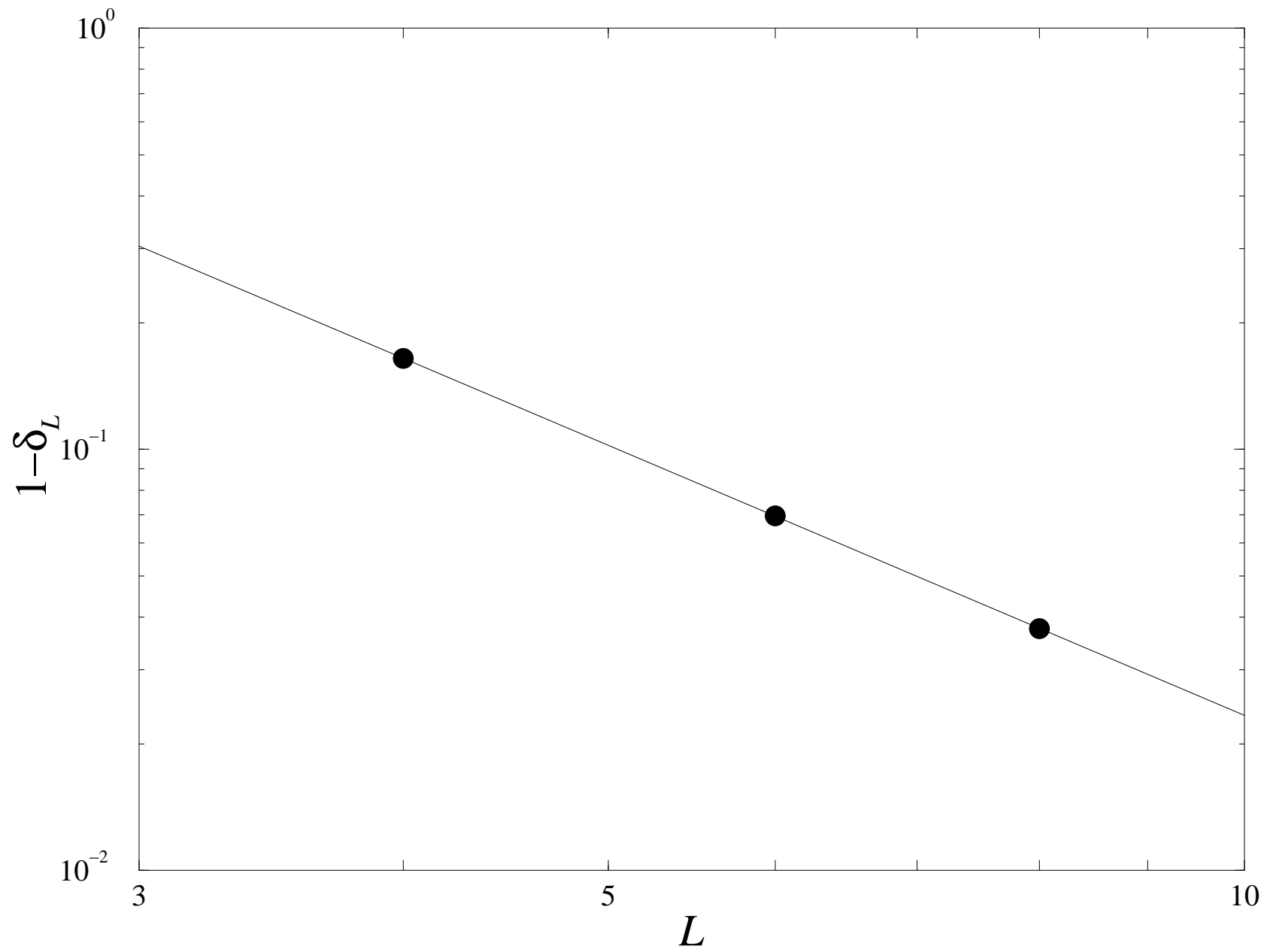


Fig. 4

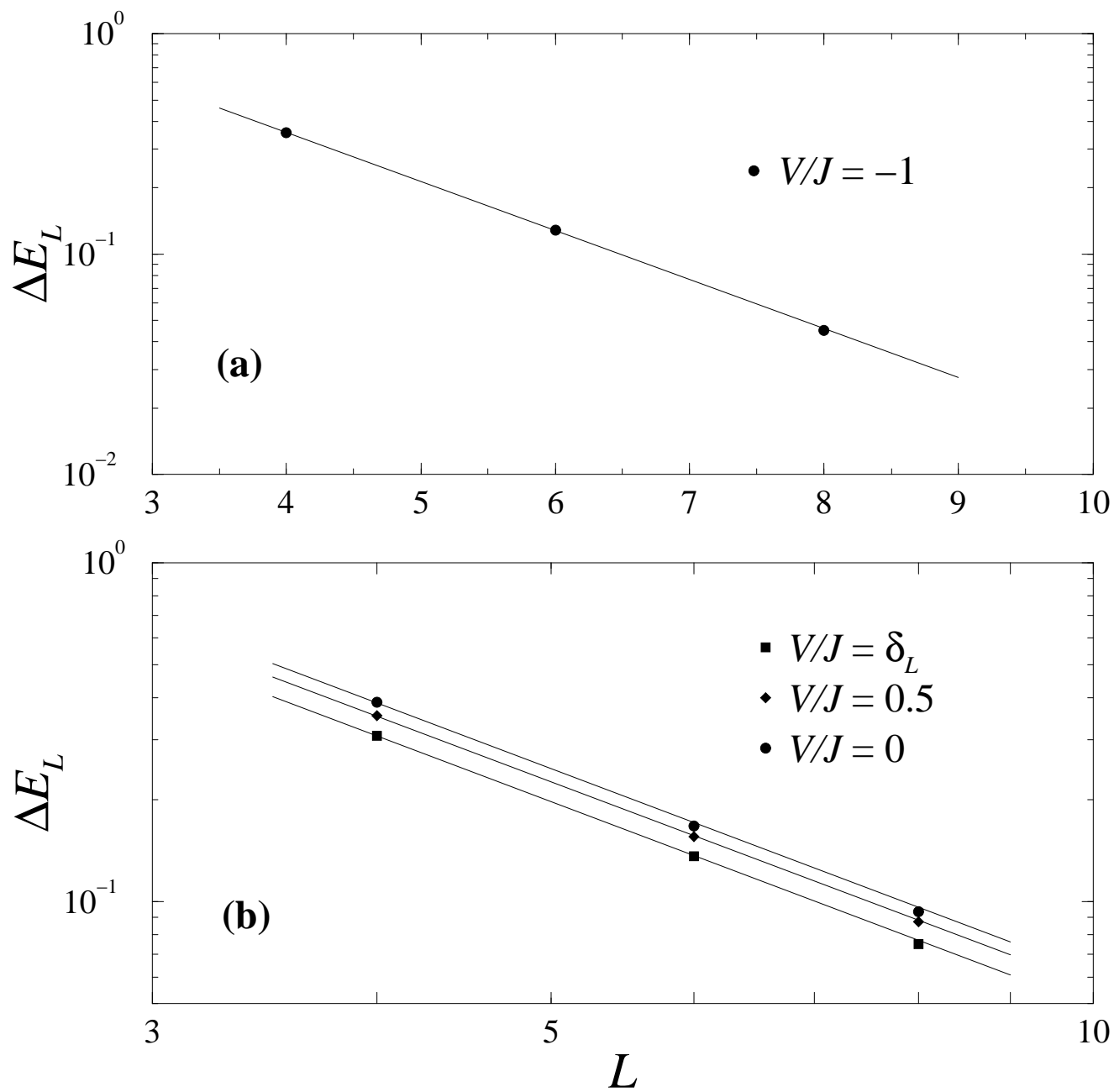


Fig. 5

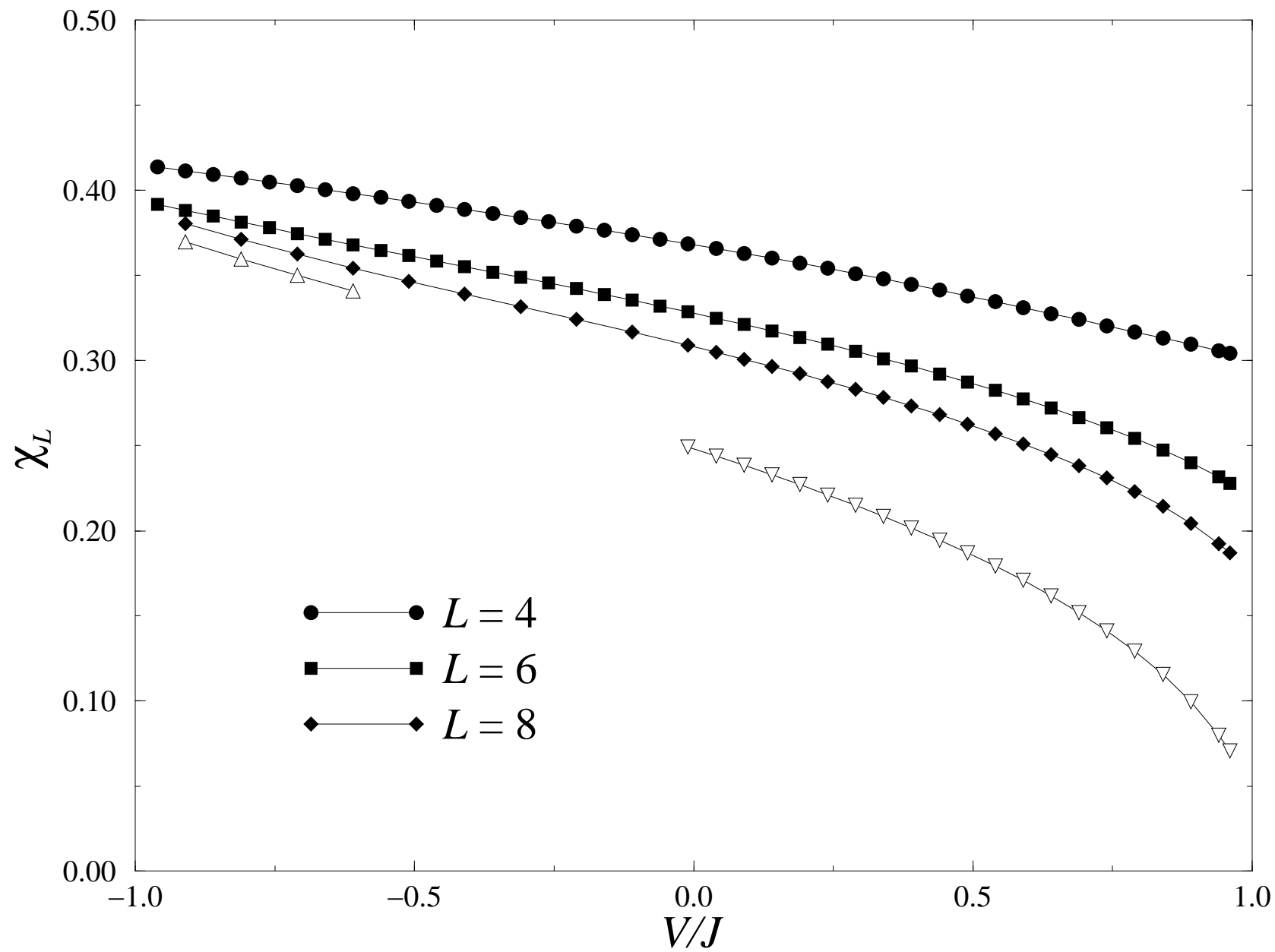


Fig. 6

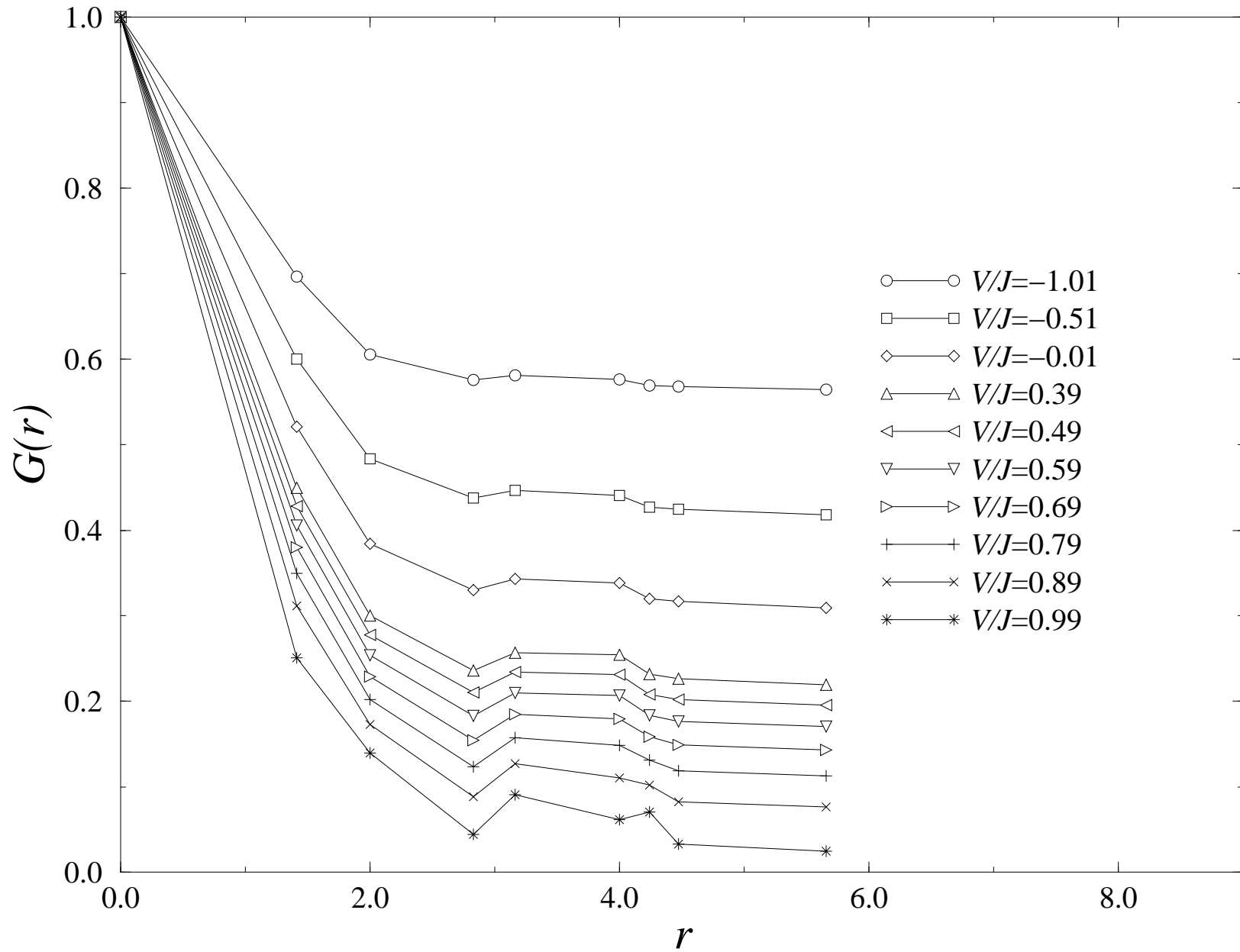
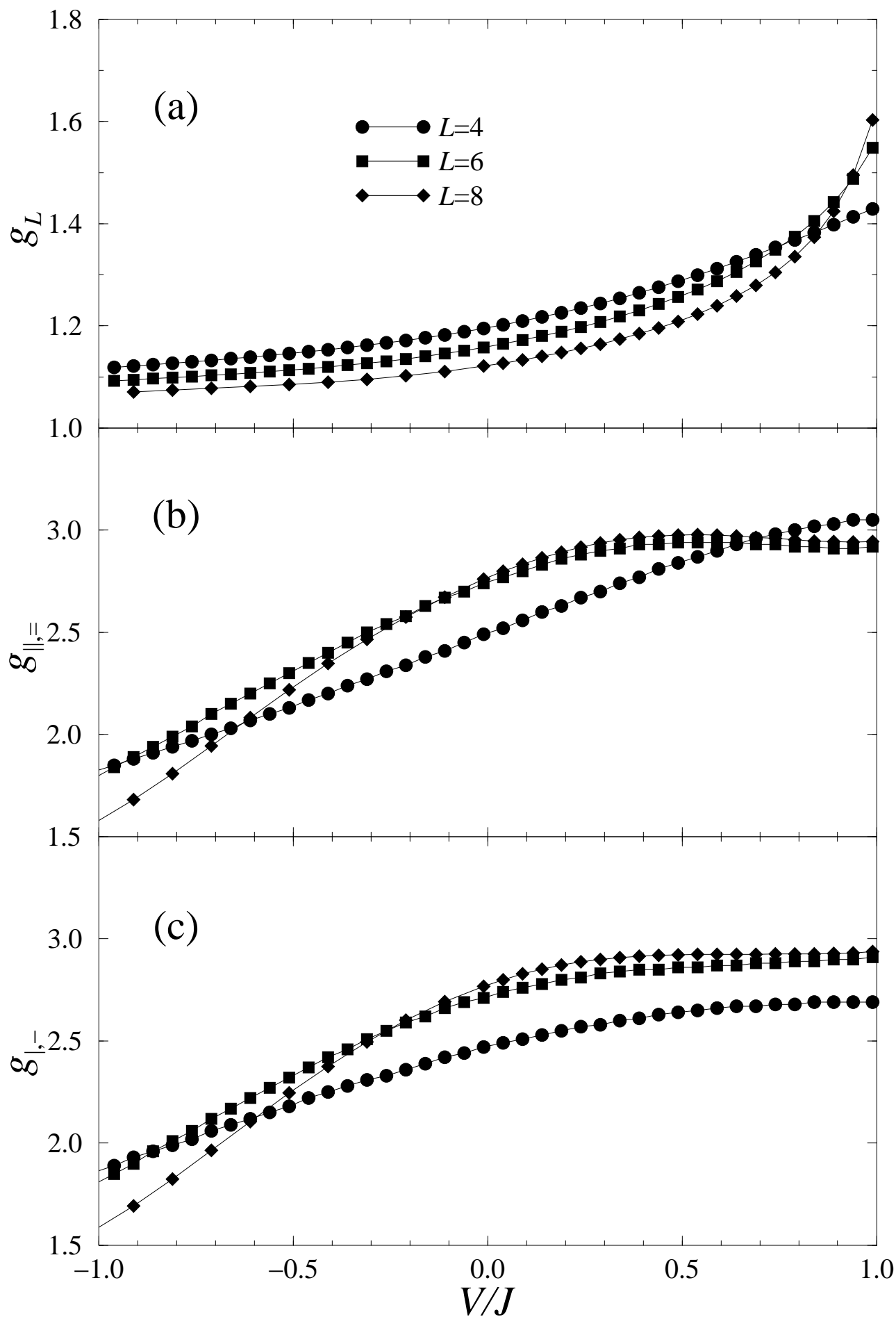
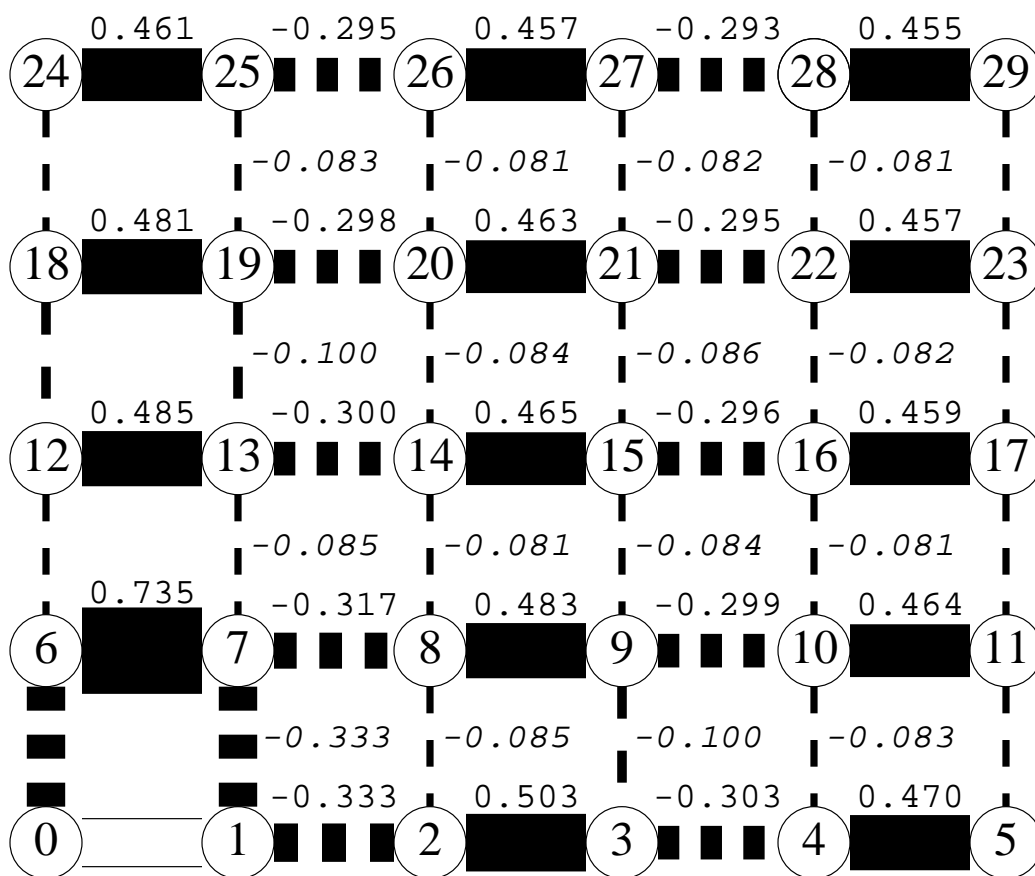


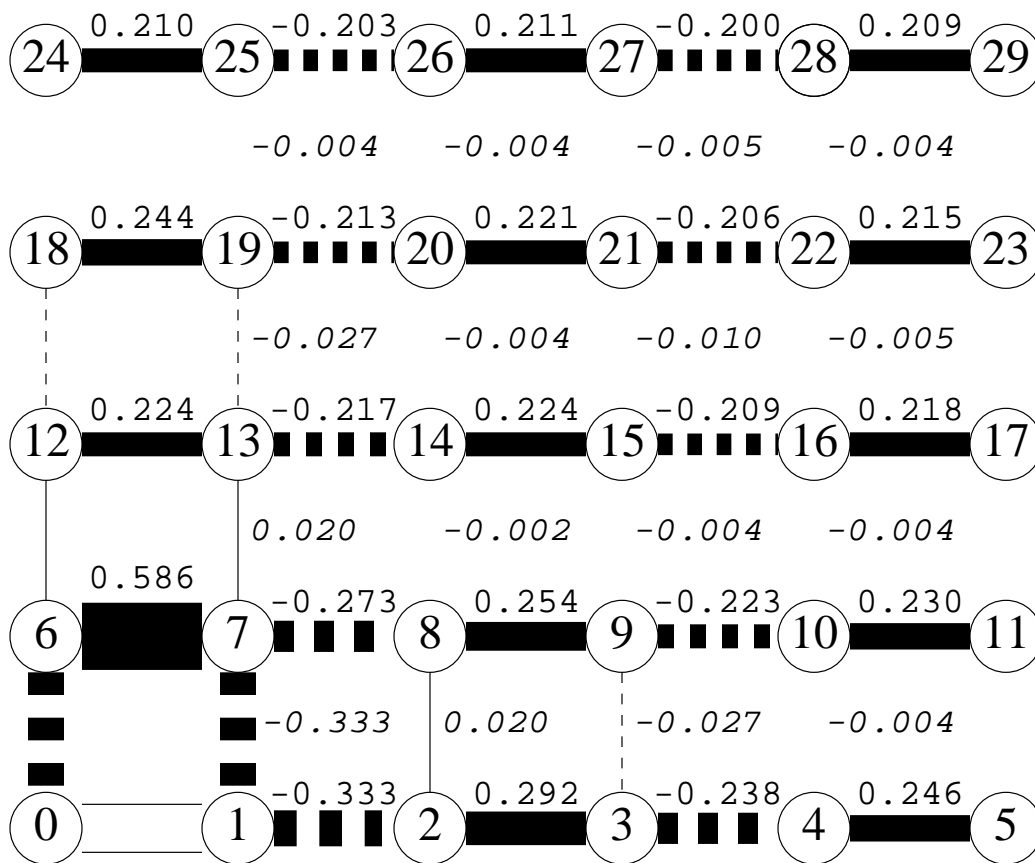
Fig. 7





(a)

Fig. 8



(b)

Fig. 8

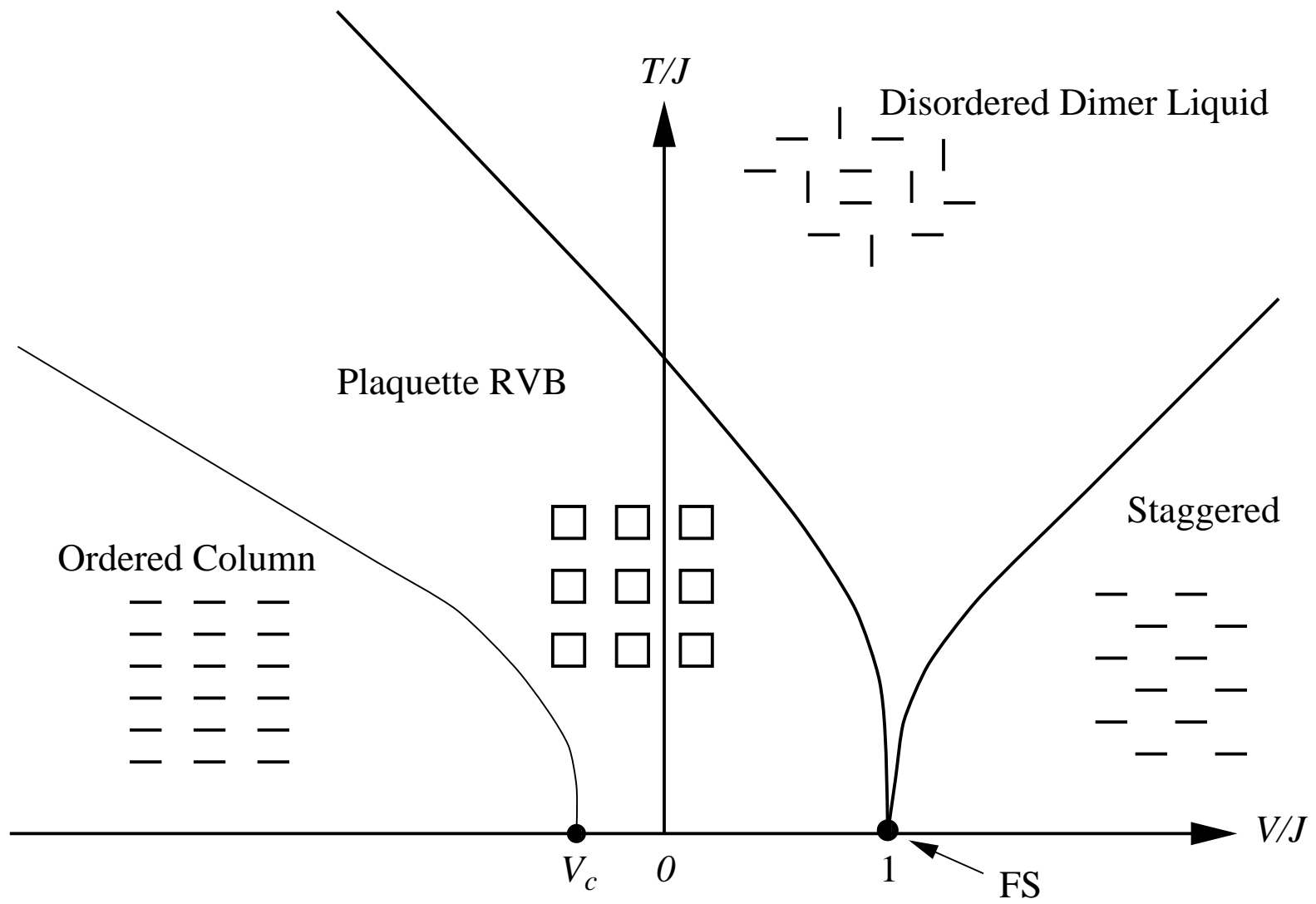


Fig. 9

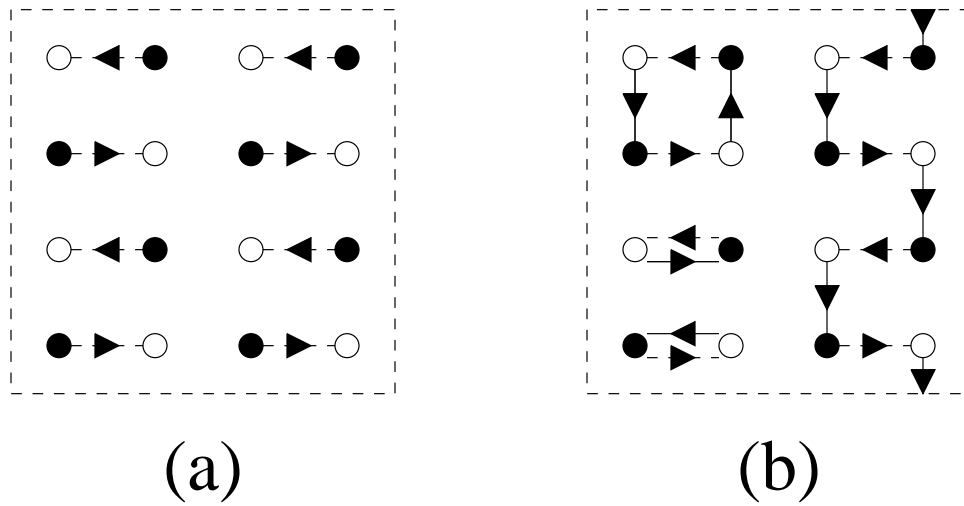


Fig. 10